On the accuracy of thin-ice thickness retrieval using MODIS thermal imagery over Arctic first-year ice

Marko MÄKYNEN, Bin CHENG, Markku SIMILÄ

Marine Research Unit, Finnish Meteorological Institute, Helsinki, Finland
E-mail: marko.makynen@fmi.fi

ABSTRACT. We have studied the accuracy of ice thickness (h_i) retrieval based on night-time MODIS (Moderate Resolution Imaging Spectroradiometer) ice surface temperature (T_s) images and HIRLAM (High Resolution Limited Area Model) weather forcing data from the Arctic. The study area is the Kara Sea and eastern part of the Barents Sea, and the study period spans November–April 2008–11 with 199 h_i charts. For cloud masking of the MODIS data we had to use manual methods in order to improve detection of thin clouds and ice fog. The accuracy analysis of the retrieved h_i was conducted with different methods, taking into account the inaccuracy of the HIRLAM weather forcing data. Maximum reliable h_i under different air-temperature and wind-speed ranges was 35–50 cm under typical weather conditions (air temperature <–20°C, wind speed <5 m s^{-1}) present in the MODIS data. The accuracy is best for the 15–30 cm thickness range, ~38%. The largest h_i uncertainty comes from air temperature data. Our ice-thickness limits are more conservative than those in previous studies where numerical weather prediction model data were not used in the h_i retrieval. Our study gives new detailed insight into the capability of T_s-based h_i retrieval in the Arctic marginal seas during freeze-up and wintertime, and should also benefit work where MODIS h_i charts are used.

INTRODUCTION

In the Arctic Ocean the ocean–atmosphere heat, momentum and gas exchanges are controlled by the sea-ice thickness distribution. Thin ice with a thickness of <0.5 m produces strong heat and salt fluxes and affects the weather and deep water circulation in the Arctic. Spaceborne remote sensing of sea-ice thickness can be conducted based on Archimedes' law and satellite radar or laser altimeter measurements of freeboard (Laxon and others, 2003; Kwok and Rothrock, 2009). However, this method results in large relative errors for thin ice (Laxon and others, 2003). Passive microwave radiometer data at frequencies of 19, 37 and 85 GHz have been used to estimate thickness of thin ice up to 10–20 cm based on correlation between ice surface salinity (i.e. dielectric properties) and ice thickness (Martin and others, 2004; Nihashi and others, 2009; Singh and others, 2011; Tamura and Ohshima, 2011). However, Nihashi and others (2009) showed that at least 37 GHz data cannot detect thin ice when that ice is covered with snow. Kaleschke and others (2012) demonstrated that lower-frequency L-band radiometer data from the Soil Moisture and Ocean Salinity (SMOS) satellite can be used to retrieve sea-ice thickness up to 0.5 m. The major drawbacks are the coarse resolution of the radiometer data, grid size of 12.5–35 km, which prevents detection of smaller leads and polynyas, and the currently poorly known effect of snow cover on the thin-ice thickness estimation.

Correlation between sea-ice thickness and synthetic aperture radar (SAR) data has also been studied. For the Baltic Sea it was demonstrated that thickness estimation of deformed ice under dry snow conditions is possible through a statistical relationship between the ice freeboard and the radar backscatter (Similä and others, 2010). The variance of the mean freeboard, i.e. large-scale surface roughness, increases with increasing mean freeboard, and, as the surface roughness increases, the backscatter also increases. Nakamura and others (2006) found good correlation between the L- (0.87) and C-band (0.80) co-polarization ratio and the thickness of undeformed ice in the Sea of Okhotsk. Good correlation has also been found between Antarctic first-year pack-ice and fast-ice thickness and the C-band co-polarization ratio (Nakamura and others, 2009). The co-polarization ratio has little sensitivity to ice surface roughness and is related to variations in salinity, i.e. ice surface dielectric constant, that can be caused by changes in ice thickness (Wakabayashi and others, 2004). Airborne C-band polarimetric SAR data together with a theoretical backscattering model have been used to estimate ice thickness in the 0–10 cm range (Kwok and others, 1995). SAR-based methods for thin-ice thickness retrieval are still experimental, and no operational products are yet available.

The final option for spaceborne thin-ice thickness (h_i) estimation is based on the ice surface temperature, T_s, from satellite thermal imagery and the ice surface heat balance equation (Yu and Rothrock, 1996). Major assumptions here are that the heat flux through the ice and snow is equal to the atmospheric flux, and snow and ice temperature profiles are linear. This method is based on the physical relationship between T_s and h_i and is well established in the literature. In addition, the microwave radiometer h_i estimation methods at frequencies of 19, 37 and 85 GHz are based on regression between the radiometer data and T_s-based h_i. The spatial resolution of T_s-based h_i charts is ~1 km, which is fine enough for detection of all polynyas and leads with equivalent width. Drawbacks here are the need for external atmospheric forcing data and cold cloud-free conditions.

Here we study h_i retrieval using Moderate Resolution Imaging Spectroradiometer (MODIS) thermal imagery, and conduct detailed analysis on the accuracy of the retrieved h_i under different air temperature (T_a) regimes in the Arctic. The study area includes the Kara Sea and the eastern part of the Barents Sea (Fig. 1). The external forcing data for solving the surface heat balance come from a numerical weather prediction (NWP) model, HIRLAM (High Resolution Limited

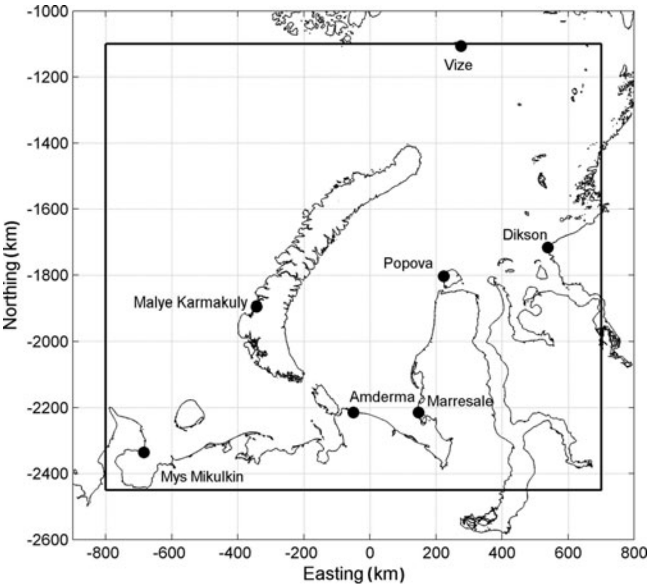

Fig. 1. Barents and Kara Seas study area for MODIS-based ice thickness retrieval. Rectangle shows the area, and dots are weather stations. Polar stereographic coordinates with mid-longitude of 63E.

Area Model) (Källen, 1996; Undén and others, 2002). The h_i estimates are obtained only from night-time MODIS data. Thus, the uncertainties related to the effect of the solar shortwave radiation and surface albedo are excluded. Snow vs ice thickness parameterization needed in the h_i retrieval was estimated from climatology and Russian Sever data (NSIDC, 2004). The cloud masking of the MODIS data was conducted using three spectral cloud tests and manual methods. Our MODIS h_i chart collection spans three winters (November–April) in 2008–11 with 199 charts.

The accuracy of the retrieved h_i is studied in the following ways:

1. Using estimated or guessed standard deviations and covariances of the input variables to the h_i retrieval, the h_i uncertainty is estimated with the Monte Carlo method. The accuracy of the HIRLAM data is studied by comparing them to coastal weather station data.

2. Thickness charts from consecutive days are compared to each other. Large differences are mainly due to the cloud-masking errors and HIRLAM data inaccuracies.

Method 2 has not been used in previous studies. Unfortunately, we do not yet have any in situ thickness data for the h_i validation. As another new method, the typical maximum reliable h_i under different T_a ranges is determined using not only the results from (1), but also the empirical mean $T_a - T_s$ vs h_i curves, which show how rapidly h_i changes as a function of a slight change in T_s or T_a. We compare our h_i accuracy results and limits for the maximum reliable h_i to previous studies.

Unlike some previous studies (e.g. Yu and Rothrock, 1996; Tamura and others, 2006; Wang and others, 2010), we use here for the first time a large MODIS dataset (nearly 200 swath images) combined with numerical weather forcing data (HIRLAM) for the h_i retrieval and accuracy analysis of h_i. We obtain uncertainty values for the weather forcing data by comparing them to the in situ weather data instead of using 'best-guess' values as in Yu and Rothrock (1996) and Wang and others (2010). For the first time, we present h_i uncertainties and maximum reliable h_i values under different T_a and wind-speed ranges. In determining the maximum h_i we take into account the sensitivity of the retrieved h_i to a T_s or T_a change, which has not been done in previous studies. Our study gives new detailed insight into the capability of T_s-based h_i retrieval in the Arctic marginal seas during freeze-up and wintertime, and should benefit work on microwave-radiometer-based thin-ice thickness retrieval where T_s-based h_i charts are used for algorithm development and validation.

DATA AND METHODS

In the following, datasets and methods used in the ice thickness chart calculation are described.

MODIS data

MODIS spectrometer data were acquired from NASA's Warehouse Inventory Search Tool (WIST) service over our study area (Fig. 1) under cold cloud-free night-time conditions in November–April 2008–11. The MODIS data consist of level 1B calibrated radiances at 1 km resolution (MOD02) and level 1A geolocation fields (MOD03). We chose to use only Terra MODIS data, as their acquisition times match those of Envisat advanced SAR (ASAR) Wide Swath Mode (WSM) images which will be combined with the MODIS data in a multisensor sea-ice thickness retrieval study by the authors. The MODIS acquisition times were 07:00–08:50 UTC (descending orbits) and 15:15–17:15 UTC (ascending orbits). After 15 March, only the afternoon MODIS data are utilized, as the sun zenith angle for the morning data becomes too low. After April, air temperature becomes too high for accurate h_i retrieval, and the sun zenith angle for the afternoon data becomes too low. The MODIS datasets with large cloud-free areas were visually identified using NASA's MOD29 product (MODIS/Terra Sea Ice Extent 5-Min L2 Swath 1 km) (Hall and others, 2007) and MODIS thermal RGB (red, green, blue) images. The total number of MODIS datasets here is 199. The MODIS data were rectified to a polar stereographic coordinate system (mid-longitude 63E, true-scale latitude 70N) with 1000 m pixel size using NASA's MODIS Swath Reprojection Tool.

MODIS RGB images

Two different RGB images were calculated from MODIS data: (1) brightness temperature bands 20 (red), 31 (green) and 32 (blue) (3.750, 11.030 and 12.020 µm), and (2) band difference 32–31, difference 31–22 and band 31 (this combination is used for the Meteosat SEVIRI (Spinning Enhanced Visible and Infrared Imager) instrument and is called NightMicrophysical). Both images are used in a manual cloud-masking procedure.

MODIS cloud mask

We used the following method for the cloud masking of night-time MODIS data. Based on a study of MODIS cloud masking (Frey and others, 2008) and our visual analysis of different cloud tests for the night-time data, we selected three cloud tests: (1) 11–3.9 µm brightness temperature difference (BTD) for low clouds, (2) 3.9–12 µm BTD for high clouds, and (3) 6.7 µm brightness temperature (BT) for high clouds. The thresholds for the tests were determined using empirical BT and BTD data for clouds and cloud-free sea ice

https://doi.org/10.3189/2013AoG62A166 Published online by Cambridge University Press

and open water. The cloud tests are performed using 10 × 10 pixel blocks (10 km × 10 km). If 10% or 20% of the block pixels are cloudy according to a cloud test, the block is labeled as cloudy. Next, morphological operations are performed to remove small isolated block groups (cloudy) and to fill isolated small holes (cloud-free). The results of the individual cloud tests are combined so that if a block is cloudy according to any cloud test then it is also cloudy in the combined mask. Clear restoration is conducted using 11 μm brightness temperature (BT11) by reasoning that if under cold conditions BT11 is >272 K it should represent cloud-free open water or very thin ice. After that, filling of the small holes is again conducted. Next, the following manual editing procedures can be conducted: filling holes, removing erroneous cloud mask elements, and masking arbitrary polygonal areas as cloudy or clear. The manual editing is conducted using the two RGB images described above. Finally, the T_s image is calculated and another round of manual cloud-mask editing is conducted using the T_s image and the two RGB images.

Our approach to the MODIS cloud masking yields a mask that is much less 'grainy' than a typical pixel-based mask (e.g. in the MOD29 product (Hall and others, 2007)). In addition, in our cloud mask, mask errors due to the MODIS sensor striping effect are not present. However, distinguishing clear sky from clouds is nowhere more difficult than in winter night-time conditions (Frey and others, 2008), and there are likely cases of unmasked thin clouds and fog in the T_s images.

MODIS ice surface temperature

The MODIS T_s under clear-sky conditions is obtained with a split-window technique, where 'split-window' refers to BTD in the 11–12 μm atmospheric window (Hall and others, 2004). This technique allows for the correction of atmospheric effects primarily due to water vapor. The root-mean-square error (RMSE) of T_s is at least 1.3 K (Hall and others, 2004).

HIRLAM

HIRLAM is a short-range NWP model (Källen, 1996; Undén and others, 2002), developed by an international consortium of 11 European countries (http://hirlam.org). HIRLAM products are not routinely available over the Arctic Ocean, so we performed dedicated HIRLAM experiments over the research domain (Fig. 1) during November–April 2008–11. The experiments were run with the HIRLAM version 7.3newsnow, which contained improved surface parameterizations, including updated schemes for predicting snow and ice. Short forecasts with a lead time up to 9 hours were initialized every 6 hours (00, 06, 12 and 18 UTC). The horizontal resolution of the experiments was 7.5 km, and the model had 60 levels in the vertical. Snow depth, sea surface temperature (SST) and ice cover analyses as well as soil temperature and moisture data assimilation were performed using optimal interpolation, based on SYNOP observations and European Centre for Medium-Range Weather Forecasts (ECMWF) SST/ice-cover analyses. Over our research domain, an average of seven SYNOP stations, located on the coastline and islands, reported surface weather observations every 3 hours. The HIRLAM upper-air analysis was replaced by an interpolation of the ECMWF analyses, which were also used as lateral boundaries for the HIRLAM experiment.

In the MODIS T_s-based h_i retrieval, the following HIRLAM model parameters are used: air temperature at 2 m height, wind speed at 10 m, relative humidity at 2 m and downward longwave radiation. The parameters at 2 and 10 m heights are diagnostic variables obtained from the HIRLAM lowest-level (~32 m) prognostic variables. In our polar stereographic coordinate system (mid-longitude 63E, true-scale latitude 70N) the HIRLAM parameters were interpolated to 20 km gridpoint spacing and to temporal resolution of 1 hour. For the h_i retrieval the HIRLAM parameters were further interpolated to the MODIS 1 km pixels using the nearest-neighbor method.

Model relating sea-ice surface temperature and level ice thickness

Level ice thickness from T_s can be estimated on the basis of a surface heat balance equation. Major assumptions here are that the heat flux through the ice and snow is equal to the atmospheric flux, and temperature profiles are linear in ice and snow (Yu and Rothrock, 1996). The heat balance equation at the top surface (whether sea ice or snow) during the night-time is (Yu and Rothrock, 1996)

$$\left(F_l^{up} + F_l^{dn} + F_s + F_e\right) + F_c = F_t + F_c = 0, \quad (1)$$

where F_l^{up} and F_l^{dn} are upward and downward longwave radiative fluxes, F_s and F_e are turbulent sensible and latent heat fluxes, and F_c is conductive heat flux approximated as

$$F_c = \gamma(T_w - T_s), \quad (2)$$

$$\gamma = \frac{k_i k_s}{k_s h_i + k_i h_s}, \quad (3)$$

where γ is the thermal conductance of the snow/ice sheet, k_i and k_s are heat conductivities of ice and snow, h_s is snow thickness and T_w is the freezing temperature of sea water approximated as $T_w = -0.054 S_w$, where S_w is the salinity of sea water. In Eqn (1), fluxes entering the top surface are positive (F_l^{dn} always), and fluxes leaving the surface are negative (F_l^{up} always).

Based on the known T_s, the surface heat fluxes and parameterized h_s, k_i and k_s, the estimation of h_i can be carried out. F_l^{up} is obtained on the basis of MODIS-derived T_s assuming constant sea-ice thermal emissivity, ε, of 0.98, and F_l^{dn} is from the HIRLAM model. F_s and F_e are calculated as in Yu and Rothrock (1996) where the bulk transfer coefficients for heat and evaporation, C_s and C_e, are assumed to be 0.003 for very thin ice and 0.00175 for thick ice. For k_s we assume a constant climatological value of 0.3 W m K^{-1} (Sturm and others, 1997). k_i is calculated using Untersteiner's (1964) equation and estimating ice bulk temperature, T_i, with T_s as was done by Yu and Rothrock (1996). k_i also depends somewhat on bulk ice salinity, S_i. According to the following general expression (Kovacs, 1996),

$$S_i = 4.606 + 91.603/h_i, \quad (4)$$

S_i decreases from 13.8 ppt to 6.4 ppt when h_i increases from 10 cm to 50 cm. To simplify the h_i retrieval and to take into account that S_i is in reality a complex function of sea-water salinity, ice growth rate and desalination processes, we always use in the k_i calculation an S_i value for 30 cm thick ice (7.7 ppt). The variation of k_i as a function of S_i is very small (<10%) when $T_i < 268$ K and $h_i > 10$ cm. When T_s is close to T_w (case of very thin ice under cold conditions) then k_i decreases rapidly as a function of T_s. Thus, k_i is assumed to be constant when $T_s < 270$ K.

https://doi.org/10.3189/2013AoG62A166 Published online by Cambridge University Press

For the h_i retrieval, a relationship between h_s and h_i is needed. If it is assumed to be linear of the form

$$h_s = b_1 h_i \tag{5}$$

then h_i is calculated from

$$h_i = \frac{k_s}{k_s + b_1 k_i} H, \tag{6}$$

where H is so-called thermal ice thickness (effect of snow cover excluded),

$$H = \frac{k_i (T_s - T_w)}{F_t}. \tag{7}$$

There are a number of simplifications/approximations in the above approach, in order to minimize the difficulties in retrieving h_i. The accuracy of the approach is highly sensitive with respect to the model parameterizations and the accuracy of the forcing data. In a previous study in the Arctic it was assessed that the h_i uncertainty increases from 27% for thin ice (20 cm) to 50% for h_i around 1 m during winter night-time conditions (Yu and Rothrock, 1996). The largest uncertainties came from F_l^{dn} and F_s. It was concluded that T_s-based h_i data can resolve the regional and seasonal variations in thin ice. A more recent study, utilizing the same method of h_i retrieval as Yu and Rothrock (1996) with the Advanced Very High Resolution Radiometer (AVHRR) Polar Pathfinder extended (APP-x) product (25 km pixel size), showed h_i estimation capability up to ~2.8 m with an accuracy of >80% (Wang and others, 2010). Passive microwave sea-ice concentration data were used to correct T_s by removing the T_w contribution from overall ice-covered pixel temperature. During the night-time the largest error sources were h_s, cloud amount (related to F_l^{dn}) and wind speed. Yu and Rothrock (1996) used uncertainty estimates of the heat fluxes in the h_i accuracy analysis, but Wang and others (2010) used the variables of the heat fluxes. Neither study used NWP model data in the h_i retrieval. T_a was estimated as T_s average over a large area plus a climatological constant, and wind speed from the geostrophic wind. Tamura and others (2006) retrieved h_i using night-time AVHRR and ECMWF NWP data over an Antarctic polynya. The standard deviation of the difference between the retrieved h_i and in situ data (max h_i 0.3 m) was only 2 cm. In addition, AVHRR and ship-borne radiation thermometer-based h_i retrievals matched each other.

In general, the h_i accuracy decreases as h_i increases, and the accuracy and the maximum retrievable h_i decreases as weather gets warmer, as T_s then saturates at smaller h_i and the T_s contrast between different ice thicknesses decreases. The above approach for T_s-based h_i retrieval is only valid for smooth thermodynamically grown ice.

Coastal weather station data

There are seven coastal weather stations in our study area (Fig. 1). Weather observations were conducted at 0, 6, 12 and 18 h UTC. Air temperature at 2 m, wind speed at 10 m and relative humidity at 2 m are used to study the accuracy of the HIRLAM model data.

RESULTS AND DISCUSSION

The construction of the MODIS T_s-based ice thickness chart starts with the determination of a statistical relationship between h_s and h_i. Next, the accuracy of the HIRLAM forcing data needed in the MODIS T_s-based h_i retrieval is studied. This is followed by presentation of the MODIS h_i charts, and detailed accuracy analysis of the h_i charts with different methods. Typical maximum reliable h_i is also estimated.

Statistical relationship between snow and ice thickness

Yu and Rothrock (1996) used an empirical relationship between h_s and h_i by Doronin (1971) in retrieving h_i from the AVHRR data:

$$\begin{aligned} h_s &= 0 \text{ for } h_i < 5\text{ cm} \\ h_s &= 0.05\, h_i \text{ for } 5\text{ cm} \le h_i \le 20\text{ cm} \\ h_s &= 0.1 h_i \text{ for } h_i > 20\text{ cm}. \end{aligned} \tag{8}$$

We utilize snow and ice thickness data from the Soviet Union's airborne Sever expeditions (NSIDC, 2004) conducted in 1950–89 to determine the relationship between h_s and h_i. The Sever data represent late-winter conditions before the start of sea-ice melt. To estimate the h_s vs h_i relationship, we use only the so-called runway data up to h_i = 100 cm, which represent level ice, from a geographical area extending 200 km from the borders of our study area (Fig. 1). Data acquired after the end of April are not used, as this time period is not included in the MODIS datasets. The total number of data points is 322. The data amount for h_i < 40 cm is very small, only 23 data points. The linear regression fit to the data is

$$h_s = 0.049 h_i + 3.3\text{cm}. \tag{9}$$

The coefficient of determination, r^2, is very small, only 0.04, but the p-value is 0.00, due to the large data scatter. Typically h_s < 10 cm regardless of h_i. Using Eqn (9), h_s = 4.3 cm when h_i = 20 cm, whereas Eqn (8) yields h_s of only 1 cm. For ice thinner than 40 cm, Eqn (9) likely gives snow covers that are too thick.

Due to the small number of data and the large scatter of data points when h_i ≤35 cm, these data points probably do not have a large effect on the regression coefficients, as the few data points effectively cancel out each other's influence on the regression line. This was verified by fitting the regression line to data points with h_i > 35 cm. The results were equal to Eqn (9), indicating a robust fit to the dataset, particularly in this ice thickness range. Consequently, we combine the Sever data and Eqn (8) as follows: (1) the Sever data are divided into 10 cm thickness bins centered from 30 cm to 90 cm, and the mean h_s and h_i are calculated; (2) at h_i values of 0, 10 and 20 cm, Eqn (8) is used; and (3) linear regression is fitted to these data points (Fig. 2). The regression fit is

$$h_s = 0.09 h_i + 0.1\text{cm}. \tag{10}$$

The constant term is so small that it can be dropped. When h_i < 20 cm, Eqn (10) likely gives snow cover that is too thick, especially for polynyas. Thus, for this thickness range we use Eqn (8), yielding the following final h_i vs h_s relationship

$$\begin{aligned} h_s &= 0 \text{ for } h_i < 5\text{ cm} \\ h_s &= 0.05 h_i \text{ for } 5\text{ cm} \le h_i \le 20\text{ cm} \\ h_s &= 0.09 h_i \text{ for } h_i > 20\text{ cm}. \end{aligned} \tag{11}$$

The only difference between Eqns (11) and (8) is a 10% smaller slope term in Eqn (11) when h_i > 20 cm.

https://doi.org/10.3189/2013AoG62A166 Published online by Cambridge University Press

HIRLAM accuracy

The accuracy of the HIRLAM air temperature, T_a^H, wind speed, u^H, and relative humidity, Rh^H, are studied by comparing them to the coastal weather station data (T_a^w, u^w, Rh^w) from seven stations (Fig. 1). We do not have in situ data to make a comparison for the HIRLAM F_l^{dn}. In the comparison the HIRLAM data (1 hour time-step) from the gridpoints over the ocean closest to the weather stations and coincident with the weather station data (6 hour time step) were used. The comparison was conducted using HIRLAM and weather station datasets for winter 2010/11 (1 October–30 April). Table 1 shows the comparison (HIRLAM minus weather station data) results: mean bias, RMSE, standard deviation (std) and their variation from station to station, and the correlation coefficient.

The overall mean bias of T_a^H is –0.9°C (T_a^H is on average 0.9°C smaller than T_a^w). The overall RMSE and std are rather high, 3.8°C and 3.7°C, but the correlation between the two T_a datasets is nonetheless 0.94. The high correlation between T_a^H and T_a^w shows the peaks and lows of air-temperature changes are captured well by HIRLAM. There is some variation of the statistics from station to station (e.g. from 2.9°C to 4.2°C for std). The mean bias increases somewhat with decreasing T_a^H: for the T_a^H ranges –10 to –5°C and –25 to –20°C, it is –0.1°C and –2.3°C, respectively. Both RMSE and std increase with decreasing T_a^H (e.g. in the above-mentioned T_a^H ranges, RMSE is 3.0°C and 4.8°C). This HIRLAM underestimation of T_a leads to underestimation of h_i, as the $T_a - T_s$ difference now resembles that of thinner ice.

These differences between the two T_a datasets could be partly due to the sea-ice mask used in the HIRLAM model. The mask only shows either open water or thick sea ice, so the atmosphere over the sea ice is always insulated from the ocean regardless of the ice thickness. In addition, a modeling study by Lüpkes and others (2008) demonstrated that, for sea-ice concentrations greater than 90%, small changes in the sea-ice fraction have a strong increasing effect on the near-surface T_a over thick ice under clear-sky conditions during polar night.

The correlation between the u datasets is much lower than for the T_a datasets, only 0.67. Because the wind speed changes at much higher temporal frequency than air temperature, the lower correlation between u^H and u^w does not indicate a weak modeling skill by the HIRLAM as our closer analysis showed. The overall mean bias of u^H is –1.2 m s^{-1}, std is 3.1 m s^{-1} and RMSE is 3.3 m s^{-1}. These std and RMSE values indicate >100% uncertainties (std(u^H)/u^H) for u^H at lower wind speeds. Thus, the std of $u^H - u^w$ was also studied as a function of u^H. Std increases rapidly with increasing u^H up to 12 m s^{-1}, but at the same time the u^H uncertainty decreases from >100%, when $u^H \leq 2$ m s^{-1}, to ~40%. When $u^w > 9$ m s^{-1}, HIRLAM mostly underestimates it. At low u^w (<3 m s^{-1}), by contrast, HIRLAM slightly overestimates it. During the acquisitions of the MODIS datasets, u^w was typically small: in the 2010–11 data the average was 5 m s^{-1} in the Kara Sea. The HIRLAM underestimation of u leads to underestimation of absolute values of F_s and F_e which are linear functions of u. This in turn leads to either h_i overestimation if $F_s + F_e < 0$, or underestimation if $F_s + F_e > 0$.

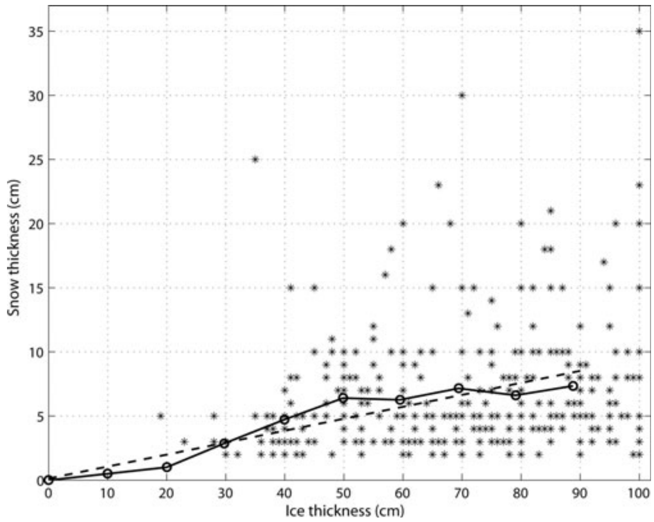

Fig. 2. The relationship between snow and ice thickness for level ice. Stars are the Sever data acquired in 1950–89 in our study area. The solid–dotted line is the average snow and ice thickness relationship using the Sever data for thickness range 30–90 cm and Doronin's (1971) empirical equation for 0–20 cm range. Dashed line is linear regression fit to the average data.

The overall mean bias and std for $Rh^H - Rh^w$ is +8% and 12%, respectively. There is no correlation between the Rh datasets. HIRLAM significantly overestimates Rh when $Rh^w < 80\%$. Rh is the input parameter only for the turbulent latent flux, F_e, whose contribution to the heat balance equation (1) is the smallest. In some previous studies, Rh has been simply assumed to be constant: 90% in Yu and Rothrock (1996) and Wang and others (2010).

For the std of the HIRLAM F_l^{dn} we assume a value of 20 W m^{-2} based on a study where different F_l^{dn} schemes were compared to in situ F_l^{dn} measurements on Baltic Sea ice (Zhang and others, 2006).

MODIS ice thickness chart

In calculating the MODIS h_i charts, the following restrictions and procedures are applied: (1) The MODIS sensor scan angle (max 55°) of the T_s data is limited to be <40° in order to restrict the effect of atmosphere and deterioration of

Table 1. Comparison between seven weather stations and HIRLAM data (HIRLAM minus station) for air temperature, T_a (°C)), wind speed, u (m s^{-1}), and relative humidity, Rh (%). The time period is 1 October 2010 to 31 April 2011

Parameter	Mean bias		RMSE		std		Correlation
	Overall	Variation	Overall	Variation	Overall	Variation	
T_a	–0.9	–2.1 to +1.0	3.8	3.1–4.7	3.7	2.9–4.2	0.94
u	–1.2	–2.4 to +0.7	3.3	2.4–4.6	3.1	2.2–3.9	0.67
Rh	+8	+1 to +15	15	11–18	12	9–13	–0.02

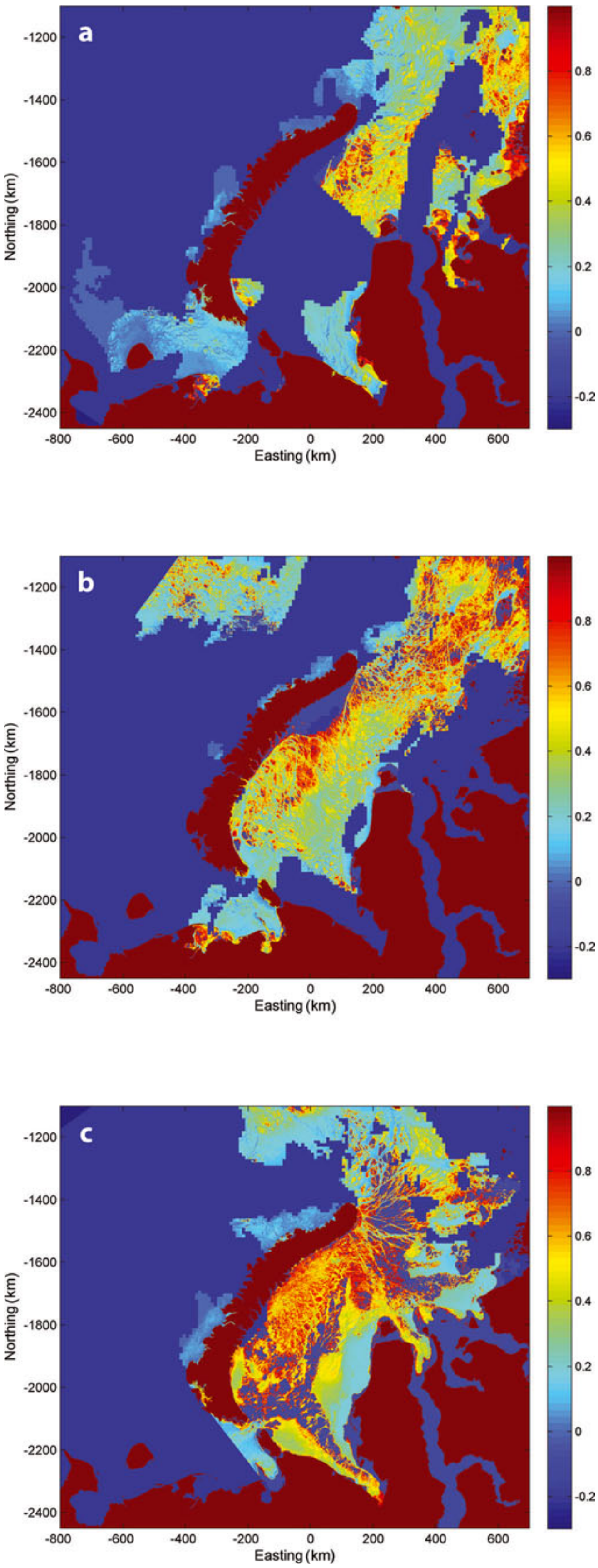

Fig. 3. Ice thickness charts derived from the MODIS ice surface temperature images acquired on (a) 31 December 2009, (b) 14 January 2010 and (c) 23 February 2010. Dark blue is either cloud (thickness –0.2 m), no data mask (–0.3 m) or scan angle mask (–0.2 m), and light blue (–0.1 m) indicates areas where ice thickness retrieval was unsuccessful or resulted in thickness values more than 1 m. Polar stereographic coordinates with mid-longitude of 63E.

spatial resolution. At a scan angle of 40° the across-track resolution is ~2 km (at nadir it is 1 km). (2) The calculated h_i is rounded to 1 cm resolution. (3) The h_i retrieval yields sometimes erroneous negative h_i values for thick ice ($F_t > 0$ in Eqn (7) which is erroneous) due to errors either in the HIRLAM data or in the model parameterizations. These erroneous h_i values are flagged in the h_i chart. (4) For very thin ice (few cm), negative h_i values are sometimes obtained; these are marked to 0 m (i.e. open water). (5) Using 10×10 km block averages of T_s and T_a the following changes are made to the calculated h_i chart: (a) If $T_a > -5$°C then the calculated h_i is masked away. It is assumed that at these high air temperatures the sensitivity of h_i to T_s is too small for accurate h_i retrieval. (b) If $T_a > -5$°C but $T_s - T_w > -1$°C, then the block is flagged as open water. It is not possible to separate accurately open water and 1–3 cm thick ice due to the inaccuracies of the T_s and heat fluxes. (6) Finally, it is assumed that h_i values greater than 1.0 m are too unreliable and they are flagged away. Figure 3 shows examples of the calculated MODIS h_i charts.

The areal coverage percentage of the h_i charts over our study area (land excluded) varies from 5% to 45%, with an average of 19%. Here the areas of unsuccessful h_i retrieval are included, as they indicate areas of thick ice ($h_i > 1$ m), although without any thickness estimate. Due to the MODIS scan angle limitation, a totally cloud-free MODIS T_s image (none was found) would cover, on average, only 77% of the study area. The percentage of T_s pixels for which the h_i retrieval was unsuccessful varied from 0% to 79%, with an average of 18%, and it increased from November to April as sea-ice thickness in general increases during the ice season due to thermodynamic growth and deformation. The average time difference between two MODIS h_i charts is 2.4 days, and the difference varies from 0.6 to 12.4 days. The temporal coverage is worst (fewest h_i charts) for November and April due to prevailing cloud cover, and best for February and March. The h_i chart coverage is most frequent over the northeastern part of the Kara Sea (top-right quarter in Fig. 1) and less frequent over the northwestern (Barents Sea) and southwestern (Pechora Sea) parts of our study area. The cloudiness frequency is hence very closely associated with the distance to open sea.

Accuracy and maximum value of the MODIS-based ice thickness

The accuracy of the MODIS T_s-based h_i is studied in two ways: (1) Using estimated or guessed standard deviations and covariances of the input variables to the h_i retrieval, the h_i uncertainty is estimated with the Monte Carlo method. The uncertainty, or relative accuracy, is quantified with std(h_i)/mean(h_i) of the sampled h_i values. (2) h_i charts from consecutive days are compared to each other. Large differences are mainly due to the cloud-masking errors, HIRLAM data inaccuracies and the frequency and spatial distribution of open leads. The comparison estimates stability of the h_i retrieval when the true h_i change is insignificant, but the forcing data and T_s may undergo significant changes in a short period of time. Currently we do not have any coincident in situ thickness data for accuracy studies.

The typical maximum reliable h_i under different T_a ranges is determined using not only the results of the above analyses, but also an empirical mean $T_a - T_s$ vs h_i relationship which shows how rapidly h_i changes as a function of a slight change of T_s or T_a.

https://doi.org/10.3189/2013AoG62A166 Published online by Cambridge University Press

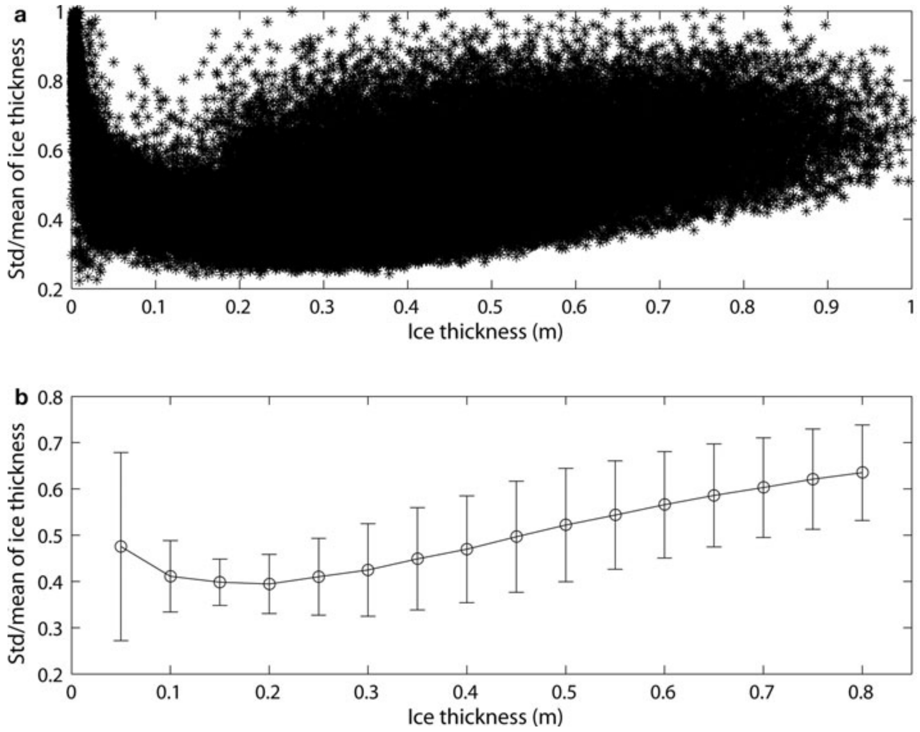

Fig. 4. Uncertainty of the MODIS-based ice thickness estimated with the Monte Carlo method. (a) Mean and std/mean of the sampled thickness values. (b) Average thickness uncertainty as a function of ice thickness and the variation of the uncertainty characterized by std(std/mean).

Ice thickness uncertainty with the Monte Carlo method

Ice thickness uncertainty with the Monte Carlo method is characterized by std(h_i)/mean(h_i), i.e. coefficient of variation (vc), of the sampled h_i values from Eqn (6). The Monte Carlo h_i sampling was conducted only at the HIRLAM gridpoints (20 km spacing), in order to reduce computation burden. T_s is here 3 by 3 pixels average at the gridpoints, to decrease local T_s variation. In total, there were 92 123 gridpoint datasets for the h_i sampling. Table 2 shows the estimated, or 'best-guess', standard deviations of the variables needed in the h_i sampling. The chosen std of 0.02 for b_1 in Eqn (11) represents 40% vc for h_s when $h_i \leq 20$ cm, and 22% when $h_i > 20$ cm. For the T_a, u and Rh, stds, instead of RMSEs, from the HIRLAM and weather station data comparison are used because the observed difference distributions are characterized by the mean bias and std. Only correlations between T_s and the HIRLAM T_a, u, Rh and F_l^{dn} are taken into account in the random sampling. These were estimated from the gridpoint data. The correlation is largest, +0.90, between T_a and F_l^{dn}, and second largest, +0.83, between T_s and T_a. For other variable combinations it varied from –0.37 to +0.78. T_s, T_a, u, Rh and F_l^{dn} were sampled from a five-dimensional normal distribution. Other variables were also sampled from normal distributions. At each gridpoint, 1000 random h_i values were calculated. Before calculating mean and std for the sampled h_i values, negative un-physical h_i values were rejected, as was the upper 5% of the positive h_i values. Very large h_i values ($h_i \gg 1$ m) are due to F_t in Eqn (7) having an expected value very close to zero and they would increase std(h_i) considerably if not excluded. Next, the h_i values were divided into 5 cm wide bins, and the mean and std of vc were calculated. The results of the Monte Carlo simulation are shown in Figures 4–6.

The mean vc with all the data is smallest, 39–41%, for the h_i range 10–25 cm and increases slowly to 64% when $h_i = 80$ cm (Fig. 4). The mean vc is 48% when $h_i = 5$ cm and approaches 100% when h_i is only 1–2 cm. If the maximum allowable mean vc is set to 50% then the typical maximum reliable h_i is ~45 cm, and the typical minimum is 4–5 cm. The large vc for very thin ice ($h_i < 5$ cm) does not matter when the h_i charts are used for ship navigation, but can be a drawback when they are used for ocean heat loss calculations.

The large scatter of data points in Figure 4 is partly due to the dependence of the h_i uncertainty on T_a and u. Figure 5 shows the mean vc as a function of T_a range. The mean vc clearly decreases with decreasing T_a when $h_i > 20$ cm. If we again take the vc limit of 50% for the reliable h_i then the maximum h_i is 60 cm when $T_a < -30$°C, but it is only 25 cm when $-20 < T_a < -15$°C. For all gridpoint data, the HIRLAM T_a is less than –20°C in 82% of cases. The mean vc as a function of u range is depicted in Figure 6. The mean vc increases considerably with increasing u when $h_i > 10$ cm.

Table 2. Standard deviations of the variables used in the Monte Carlo estimation of the MODIS-based ice thickness uncertainty

Variable	std	Variable	std
T_s	1.3 K	k_s	0.05 W m^{-1} K^{-1}
T_a	3.7 K	b_1	0.02
u	Function of u, 2.0–5.1 m s^{-1}	S_i	2 ppt
Rh	12%	ε	0.01
F_l^{dn}	20 W m^{-2}	C_s, C_e	10% of expected value

https://doi.org/10.3189/2013AoG62A166 Published online by Cambridge University Press

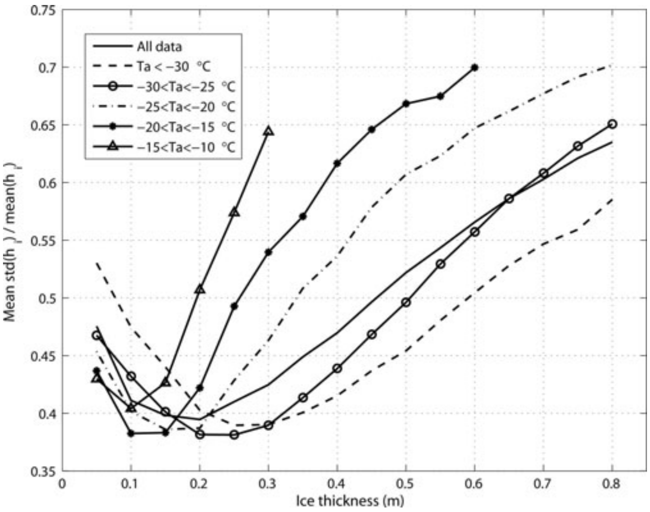

Fig. 5. Average uncertainty of the MODIS-based ice thickness as a function of HIRLAM air temperature range.

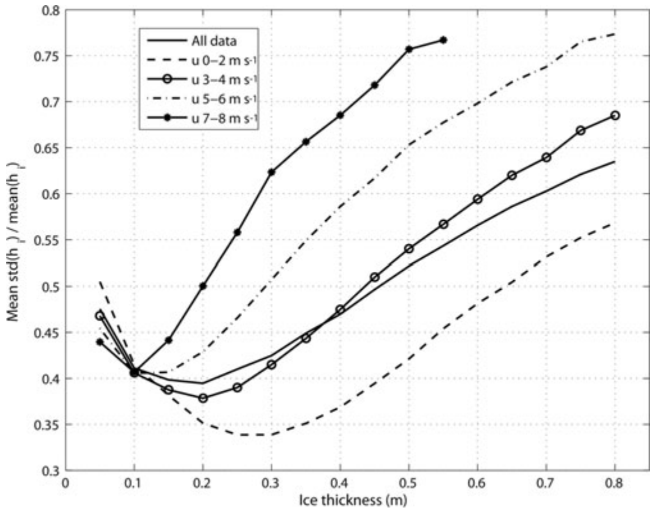

Fig. 6. Average uncertainty of the MODIS-based ice thickness as a function of HIRLAM wind-speed range.

With the 50% h_i uncertainty limit, the maximum h_i is 65 cm when $u \leq 2\,\mathrm{m\,s^{-1}}$ and only 20 cm when $7 \leq u \leq 8\,\mathrm{m\,s^{-1}}$. For the gridpoint data, the HIRLAM modal u is $3\,\mathrm{m\,s^{-1}}$ and 83% of the u values are $<5\,\mathrm{m\,s^{-1}}$. Figures 5 and 6 show that the h_i uncertainty is smallest under very cold calm wind conditions. As the h_i uncertainty depends considerably on T_a and u, it is difficult to determine the typical maximum for h_i, but under typical weather conditions ($T_a < -20°\mathrm{C}$, $u \leq 5\,\mathrm{m\,s^{-1}}$) for the MODIS data the maximum is ~50 cm. The accuracy is best for the 15–30 cm thickness range, ~38%.

The h_i uncertainty values obtained here are larger than those by Yu and Rothrock (1996). They assessed that the h_i uncertainty increases from 27% for 20 cm thick ice to 50% for h_i around 1 m. However, they estimated much smaller std for T_a and u, only 1.6°C and $0.7\,\mathrm{m\,s^{-1}}$, respectively. If we decrease std to 1°C and $1\,\mathrm{m\,s^{-1}}$ then the h_i uncertainty is <40% when $h_i = 80$ cm, and in the 10–30 cm range it is only ~22%. When the std of b_1 is doubled to 0.04, corresponding to 68% and 44% h_s uncertainty when $h_i \leq 20$ cm and $h_i > 20$ cm, respectively, the h_i uncertainty increases slightly, a 50% limit being reached when $h_i = 45$ cm. The contribution of different variables to the h_i uncertainty was studied by taking into account std of only one variable at a time in the h_i sampling. The largest h_i uncertainty comes from T_a. T_s and F_l^{dn} have somewhat smaller roughly equal contributions. When $h_i < 30$ cm then u also makes a significant contribution to the h_i uncertainty. The h_i uncertainty from snow thickness alone is ~10%. Direct comparison of our results to those of Yu and Rothrock (1996) and Wang and others (2010) is not possible as they did not use NWP model data in the h_i retrieval, but in their results F_l^{dn} and u were among the largest error sources.

Comparison of thickness maps from consecutive days

The comparison of h_i charts from consecutive days estimates the stability of h_i retrieval when the true h_i change is insignificant, but the forcing data and T_s may undergo large changes in a short period of time. Large h_i differences are mainly due to the cloud-masking errors, HIRLAM data inaccuracies and the frequency and spatial distribution of open leads. Undetected high thin clouds result in a cold bias in T_s, making the ice appear thicker than it actually is (Martin and others, 2004; Tamura and others, 2006). Ice fog generated by intense vapor flux from leads and polynyas under cold conditions is warmer than surrounding fast- or pack-ice T_s and colder than T_s for thin ice. This leads to h_i underestimation for pack ice and overestimation for thin ice. Hence, the presence of open leads has an unfavorable equalizing effect on the h_i values. The highest lead activity is also usually associated with relatively high wind speeds, which additionally weakens the retrieval accuracy.

For this study, there are 108 h_i chart pairs. The time difference between the charts varies from 15 to 33 hours, with an average of 24 hours. During these short time periods the ice growth is typically only a few centimeters (Leppäranta, 1993). h_i differences from the chart pairs were calculated using 10×10 km block averages in order to diminish the effect of ice movement. For a block with all h_i pixels valid, ($0 \leq h_i < 1$ m), std(h_i)/mean(h_i) was required to be <20% to reject ice areas in the comparison that were too heterogeneous. In total, there were 31 560 h_i difference values from the chart pairs.

The overall root-mean-square difference (RMS) for the h_i difference data is 8.5 cm, the mean absolute bias is 6.1 cm, and 90% of the absolute h_i differences are <14 cm. Within the h_i chart pairs, RMS varies from 2.1 to 19.7 cm and the average is 8.3 cm. There are no correlations between the h_i and T_a or u differences, but the absolute T_a and u differences are typically small, below 2°C and $2\,\mathrm{m\,s^{-1}}$, respectively. This suggests that cloud-masking errors caused the large RMS for some h_i chart pairs. For the h_i intervals 0–10, 10–20, 20–30, 30–40, 40–50 and 50–60 cm, RMS is 4.2, 4.9, 8.4, 9.3, 11.0 and 11.7 cm, respectively. RMS is 21–32% of the h_i bin centre value when the 0–10 cm bin is excluded. These statistics demonstrate good stability (or repeatability) of the MODIS and HIRLAM data-based h_i charts.

Maximum reliable ice thickness

Next, typical maximum reliable h_i under different T_a ranges (width 5°C) is studied using empirical mean $T_a - T_s$ vs h_i curves, which show how rapidly h_i changes as a function of a slight change in T_s or T_a. These curves were calculated from the T_s, h_i and T_a averages (3×3 pixel block) at the HIRLAM gridpoints. As $T_a - T_s$ vs h_i also depends on u it

https://doi.org/10.3189/2013AoG62A166 Published online by Cambridge University Press

was required to be <5 m s^{-1} to include only the most common wind conditions of the MODIS data. The number of gridpoint datasets was 72 955. Figure 7 shows the mean $T_a - T_s$ vs h_i curves for six different T_a ranges. The mean h_i in the curves was calculated inside 1°C wide $T_a - T_s$ bins.

When $T_a - T_s$ approaches 0°C, the sensitivity of h_i to $T_a - T_s$ increases: a 1°C change in $T_a - T_s$ can cause >10 cm change in h_i. Taking into account the RMSE of T_s and T_a (and other variables in Eqn (6)), this sensitivity is too large for accurate h_i retrieval, whereas when $T_a - T_s = -5$°C, a 1°C change leads at maximum to a 4 cm change in h_i. Not only the maximum acceptable $T_a - T_s$ vs h_i sensitivity, but also the $T_a - T_s$ difference itself may be a limiting factor for the maximum reliable h_i. When $T_a - T_s > 0$°C, then, due to the radiative surface cooling, the snow/ice surface is colder than the air and the simple parameterizations of the turbulent sensible and latent heat fluxes may be liable to large errors, a common problem for the stable boundary layer (Hanna and Yang, 2001; Järvenoja, 2005). We suggest that the maximum allowed $T_a - T_s$ should be 0°C or only few degrees higher. Figure 7 shows that at a fixed $T_a - T_s$ value the corresponding mean h_i decreases considerably with increasing T_a.

In summary, the maximum reliable h_i depends on (1) maximum acceptable $T_a - T_s$ vs h_i sensitivity, (2) maximum allowed $T_a - T_s$, (3) acceptable h_i uncertainty based on the Monte Carlo simulation, and (4) T_a. If we set the maximum $T_a - T_s$ to 0°C and the $T_a - T_s$ vs h_i sensitivity to be <10 cm °C^{-1}, then the maximum h_i varies from 50 cm when $T_a < -30$°C (max $T_s - T_a$ now –2°C due to the sensitivity limit) to 35 cm when $-20 \leq T_a < -15$°C (max $T_a - T_s = 0$°C). For the first T_a range, the h_i uncertainty is <50%, but for the second one the 50% uncertainty limit decreases the maximum h_i to 25 cm. Combining the results, the typical maximum reliable h_i is ~35–50 cm under typical weather conditions ($T_a < -20$°C, $u \leq 5$ m s^{-1}) present in the MODIS data.

CONCLUSIONS

We have studied ice thickness retrieval in the Kara Sea and eastern part of the Barents Sea using night-time MODIS T_s images and HIRLAM weather forcing data, and conducted detailed accuracy analysis of the retrieved h_i for ice <1 m thick. For the cloud masking of the MODIS data we had to use manual methods in order to improve detection of cloud-covered areas, mainly thin clouds and ice fog. These manual methods are not suitable for processing a large number of MODIS images (too time-consuming) or to be included in an operative MODIS h_i chart processing chain.

Our MODIS h_i chart collection of 199 charts spans three winters (November–April) in 2008–11. The temporal coverage of the charts is worst for November and April due to prevailing cloud cover, and best for February and March. Over the northwestern (Barents Sea) and southwestern (Pechora Sea) parts of our study area (Fig. 1) the temporal and spatial h_i chart coverage is typically too small to follow development of thin-ice areas (leads, polynyas).

We conducted detailed accuracy analysis of the retrieved h_i using three different methods, taking into account the inaccuracy of the HIRLAM weather forcing data, and determined maximum reliable h_i values under different T_a and u ranges. The typical maximum reliable h_i is 35–50 cm under typical weather conditions ($T_a < -20$°C, $u \leq 5$ m s^{-1}) present in the MODIS data. The accuracy is best for the

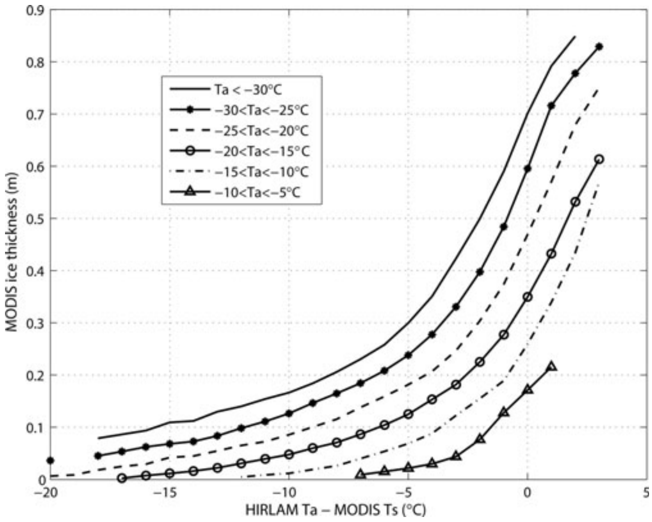

Fig. 7. Empirical average relationship between the HIRLAM air temperature and MODIS ice surface temperature difference and the retrieved ice thickness for different air temperature ranges.

15–30 cm thickness range, ~38%. Our h_i limits are more conservative than those in previous studies (Yu and Rothrock, 1996; Wang and others, 2010) where NWP model data were not used in the h_i retrieval. The large difference from the maximum h_i of 2.8 m estimated by Wang and others (2010) is likely also due to the APP-x dataset (25 km pixel size, T_s corrected with ice concentration data) used in that study. A straightforward way of increasing the accuracy of our MODIS-based h_i is to increase the accuracy of the NWP forcing data, if possible. Further studies include h_i retrieval using snow thickness information from microwave radiometer data or from a sea-ice thermodynamic model, and the effect of the ice deformation derived from SAR data on the h_i accuracy.

Our results give new detailed insight into the capability of T_s-based h_i retrieval in the Arctic marginal seas during freeze-up and wintertime, and should also benefit work on microwave-radiometer-based h_i retrieval where T_s-based h_i charts are used for algorithm development and validation.

REFERENCES

Doronin YuP (1971) *Thermal interaction of the atmosphere and the hydrosphere in the Arctic.* Israel Program for Scientific Translations, Jerusalem

Frey RA and 6 others (2008) Cloud detection with MODIS. Part I: Improvements in the MODIS cloud mask for Collection 5. *J. Atmos. Oceanic Technol.*, **25**(7), 1057–1072 (doi: 10.1175/2008JTECHA1052.1)

Hall DK, Key J, Casey KA, Riggs GA and Cavalieri DJ (2004) Sea ice surface temperature product from MODIS. *IEEE Trans. Geosci. Remote Sens.*, **42**(5), 1076–1087 (doi: 10.1109/TGRS.2004.825587)

Hall DK, Riggs GA and Salomonson VV (2007) (updated daily) *MODIS/Terra Sea Ice Extent 5-Min L2 Swath 1km, Version 5.* National Snow and Ice Data Center, Boulder, CO. Digital media: http://nsidc.org/data/mod29v5.html [Nov–Apr, 2008–2011]

Hanna SR and Yang R (2001) Evaluations of mesoscale models' simulations of near-surface winds, temperature gradients, and mixing depths. *J. Appl. Meteorol.*, **40**(6), 1095–1104 (doi: 10.1175/1520-0450(2001)040<1095:EOMMSO>2.0.CO;2)

Järvenoja S (2005) Problems in predicted HIRLAM T2m in winter, spring and summer. In *Proceedings of 4th SRNWP/HIRLAM*

Workshop on Surface Processes, Surface Assimilation and Turbulence, 15–17 September 2004. Norrköping, Sweden. Swedish Meteorological and Hydrological Institute, Norrköking, 14–26 http://srnwp.met.hu/workshops/Norrkoping_2004/index.htm

Kaleschke L, Tian-Kunze X, Maaß N, Mäkynen M and Drusch M (2012) Sea ice thickness retrieval from SMOS brightness temperatures during the Arctic freeze-up period. *Geophys. Res. Lett.*, **39**(5), L05501 (doi: 10.1029/2012GL050916)

Källén E ed (1996) *HIRLAM documentation manual, system 2.5*. Swedish Meteorological and Hydrological Institute, Norrköping

Kovacs A (1996) Sea ice. Part 1. Bulk salinity versus ice floe thickness. *CRREL Rep.* 96-7.

Kwok R and Rothrock DA (2009) Decline in Arctic sea ice thickness from submarine and ICESat records: 1958–2008. *Geophys. Res. Lett.*, **36**(15), L15501 (doi: 10.1029/2009GL039035)

Kwok R, Nghiem SV, Yueh SH and Huynh DD (1995) Retrieval of thin ice thickness from multifrequency polarimetric SAR data. *Remote Sens. Environ.*, **51**(3), 361–374 (doi: 10.1016/0034-4257(94)00017-H)

Laxon S, Peacock N and Smith D (2003) High interannual variability in sea ice thickness in the Arctic region. *Nature*, **425**(6961), 947–950 (doi: 10.1038/nature02050)

Lepparanta M (1993) A review of analytical models sea-ice growth. *Atmos.–Ocean*, **31**(1), 123–138 (doi: 10.1080/07055900.1993.9649465)

Lüpkes C, Vihma T, Birnbaum G and Wacker U (2008) Influence of leads in sea ice on the temperature of the atmospheric boundary layer during polar night. *Geophys. Res. Lett.*, **35**(3), L03805 (doi: 10.1029/2007GL032461)

Martin S, Drucker R, Kwok R and Holt B (2004) Estimation of the thin ice thickness and heat flux for the Chukchi Sea Alaskan coast polynya from Special Sensor Microwave/Imager data, 1990–2001. *J. Geophys. Res.*, **109**(C10), C10012 (doi: 10.1029/2004JC002428)

Nakamura K, Wakabayashi H, Uto S, Naoki K, Nishio F and Uratsuka S (2006) Sea-ice thickness retrieval in the Sea of Okhotsk using dual-polarization SAR data. *Ann. Glaciol.*, **44**, 261–268 (doi: 10.3189/172756406781811420)

Nakamura K, Wakabayashi H, Uto S, Ushio S and Nishio F (2009) Observation of sea-ice thickness using ENVISAT data from Lützow–Holm Bay, East Antarctica. *IEEE Trans. Geosci. Remote Sens.*, **6**(2), 277–281 (doi: 10.1109/LGRS.2008.2011061)

National Snow and Ice Data Center (NSIDC) (2004) *Morphometric characteristics of ice and snow in the Arctic Basin: aircraft landing observations from the former Soviet Union, 1928–1989*. Compiled by I.P. Romanov. National Snow and Ice Data Center, Boulder, CO. Digital media: http://nsidc.org/data/docs/noaa/g02140_romanov_arctic_seaice/index.html

Nihashi S, Ohshima KI, Tamura T, Fukamachi Y and Saitoh S (2009) Thickness and production of sea ice in the Okhotsk Sea coastal polynyas from AMSR-E. *J. Geophys. Res.*, **114**(C10), C10025 (doi: 10.1029/2008JC005222)

Similä M, Mäkynen M and Heiler I (2010) Comparison between C band synthetic aperture radar and 3-D laser scanner statistics for the Baltic Sea ice. *J. Geophys. Res.*, **115**(C10), C10056 (doi: 10.1029/2009JC005970)

Singh RK, Oza SR, Vyas NK and Sarkar A (2011) Estimation of thin ice thickness from the advanced microwave scanning radiometer-EOS for coastal polynyas in the Chukchi and Beaufort seas. *IEEE Trans. Geosci. Remote Sens.*, **49**(8), 2993–2998 (doi: 10.1109/TGRS.2011.2123101)

Sturm M, Holmgren J, König M and Morris K (1997) The thermal conductivity of seasonal snow. *J. Glaciol.*, **43**(143), 26–41

Tamura T and Ohshima KI (2011) Mapping of sea ice production in the Arctic coastal polynyas. *J. Geophys. Res.*, **116**(C7), C07030 (doi: 10.1029/2010JC006586)

Tamura T and 6 others (2006) Estimation of thin sea-ice thickness from NOAA AVHRR data in a polynya off the Wilkes Land coast, East Antarctica. *Ann. Glaciol.*, **44**, 269–274 (doi: 10.3189/172756406781811745)

Undén P and 26 others. (2002) *The high resolution limited area model. HIRLAM-5 scientific documentation*. Swedish Meteorological and Hydrological Institute, Norrköping (Technical Report)

Untersteiner N (1964) Calculations of temperature regime and heat budget of sea ice in the central Arctic. *J. Geophys. Res.*, **69**(22), 4755–4766 (doi: 10.1029/JZ069i022p04755)

Wakabayashi H, Matsuoka T, Nakamura K and Nishio F (2004) Polarimetric characteristics of sea ice in the Sea of Okhotsk observed by airborne L-band SAR. *IEEE Trans. Geosci. Remote Sens.*, **42**(11), 2412–2425 (doi: 10.1029/JZ069i022p04755)

Wang X, Key JR and Liu Y (2010) A thermodynamic model for estimating sea and lake ice thickness with optical satellite data. *J. Geophys. Res.*, **115**(C12), C12035 (doi: 10.1029/2009JC005857)

Yu Y and Rothrock DA (1996) Thin ice thickness from satellite thermal imagery. *J. Geophys. Res.*, **101**(C11), 25 753–25 766 (doi: 10.1029/96JC02242)

Zhang Z, Cheng B, Launiainen J, Wu H and Liu Y (2006) Intercomparisons of thermodynamic sea-ice modeling results using various parameterizations of radiative flux. *Acta Oceanol. Sin.*, **25**(1), 21–31